Wavenumber Selection and Hysteresis in Nonlinear Baroclinic Flows

SHIH-HUNG CHOU

Wavenumber Selection and Hysteresis in Nonlinear Baroclinic Flows

SHIH-HUNG CHOU

Earth System Science Division, NASA/Marshall Space Flight Center, Huntsville, Alabama

(Manuscript received 19 April 1994, in final form 6 March 1995)

ABSTRACT

Wavenumber transition and hysteresis in a highly unstable baroclinic flow are investigated using a high-resolution spectral numerical model. As the flow becomes more supercritical, the dominant wave gradually shifts from the most unstable wave predicted by the linear theory to a longer wave with a larger time-averaged amplitude, while the rectified mean flow attains a stronger shear at the center of the channel. The numerical results display a complex hysteresis behavior, which occurs not only between the states of different dominant wavenumbers, but also between the states of identical dominant wavenumber but of different dynamic characteristics. In a certain parameter range three stable states, each with different dominant wavenumber, are possible, and in another parameter range four stable states are possible, among them three stable states with an identical dominant wave. The numerical results suggest that a multiple weather regime exists even without external forcing in which the flow aperiodically varies between two distinct behaviors. The effects of stable higher harmonics are assessed and it is found that their presence contributes not only to the better approximation of the model solutions but also to the selection of the final equilibrium state, due to the chaotic nature of the initial transient period.

1. Introduction

Most theories concerning the finite-amplitude behavior of unstable baroclinic waves have usually focused on the dynamics of a single wave. The restriction to a single wave is justifiable in weakly nonlinear theories since, with the assumption of small supercriticality, the dynamics for a single unstable wave become closed in a consistent way if the initial wave spectrum is also limited to that wave (e.g., Pedlosky 1970; Drazin 1972; Chou and Loesch 1986a,b). However, these theories can only be applied to a narrow range in parameter space where the deviation from marginal instability is small. The single wave restriction is sometimes justified since single wave states are frequently observed in annulus experiments, although it is unclear whether the observed wave represents the linearly most unstable wave. This wave scale probably dominates the wave spectrum at the initial growing stage, but there is no reason to believe that, as the zonal flow is altered by the growing unstable waves, it will remain dominant at finite amplitude. As the flow becomes more supercritical, linear theories predict that the fastest growing wave may gradually shift to a shorter wave. In contrast, laboratory experiments and weakly nonlinear theories have shown that the long wave may grow at the expense of the linearly most unstable wave and eventually become dominant at finite amplitude.

Another fundamental problem in geophysical-related fluid dynamics is the presence of hysteresis. In general, hysteresis occurs when, for some points in parameter space, different fluid behavior can be observed depending on the initial conditions of the experiment. Once the flow settles in a particular behavior, it remains in that state beyond the point in parameter space where it first developed. Hysteresis has been observed in the axisymmetric to wave regime transition (Fein 1973; Miller and Butler 1991). It has also been observed inside the wave regime and is usually associated with wavenumber selection, where the wavenumber observed varies with initial condition.

The presence of hysteresis and wavenumber transition in a thermally driven rotating annulus has been shown by Buzyna et al. (1978), when the imposed temperature contrast is varied gradually. This study inspired Pedlosky (1981) to analytically investigate the weakly nonlinear dynamics of wave ensembles in the limit of small Froude number, weak viscosity, and long waves, using a two-layer model on an f plane. His results show that in the case of free unstable waves the wave realized at finite amplitude is not the linearly most unstable wave. Rather, a long wave, capable of achieving the single largest steady amplitude, is favored in the competition for the potential energy of the basic state. The presence of conjugate waves, which are capable of achieving identical final amplitude, implies the presence of hysteresis. Hart (1981) in his laboratory experiment containing two layers of immiscible fluid in a rotating frame shows that there is a succession of

---

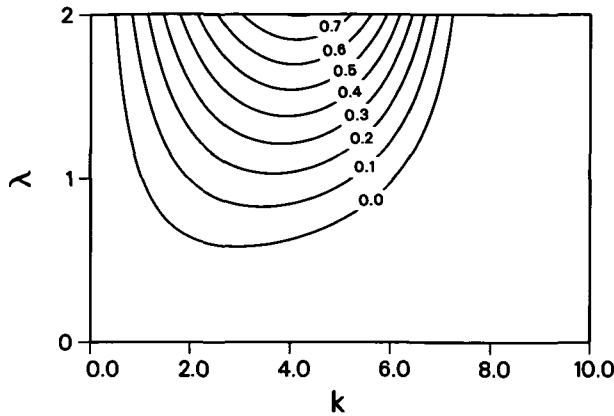*Corresponding author address:* Dr. Shih-Hung Chou, NASA/Marshall Space Flight Center, ES42, Huntsville, AL 35812.

FIG. 1. Linear growth rate as a function of wavenumber k and vertical shear λ for $S = 0.1$, $r = 1$, and $r_1 = 0.1$.

wavenumber transition to longer waves as the system becomes more supercritical. He constructed a simple analytical model that consists of only two adjacent unstable waves closed to the intersection of their marginal curves to interpret his laboratory results. Through weakly nonlinear interactions between these waves and the mean flow, either one of these waves may become dominant at the expense of the other, or the waves may coexist. These results explained reasonably well the wavenumber transition in the immediate vicinity of the intersection point of two marginal curves for adjacent wavenumbers, but observations of annulus experiments showed that the wavenumber transition may not be limited to that region.

Recently, a numerical study of wavenumber selection in a rotating, differentially heated annulus flow system was conducted by Lu et al. (1994) using a three-dimensional fully nonlinear model. Starting with an *identical* initial condition for each run, the equilibrated flow behavior displays a variety of complex fluid behavior as the outer parameter (in this case, rotation rate) is changed. The wavenumber transition regimes (which are characterized by one or more of the following behaviors: wave dispersion, two-stage equilibration, and irregular wavenumber selection) and the regular wave regimes (which equilibrates to a state consisting of only one wave and its higher harmonics) are identified. Due to the "quiescent-start" initial condition, the hysteresis region in Lu et al. (1994) is not well defined. Nevertheless, the presence of multiple solutions for certain parameter settings is evident.

The purpose of this study is to study wavenumber selection and hysteresis in an unstable baroclinic flow using a high-resolution spectral model, which includes waves both longer and shorter than the linearly most unstable wave to allow for both upscale and downscale energy transfers. Section 2 describes the model setup and its linear properties. Section 3 describes the spectral numerical technique used in solving the governing

equations. The effects of linearly stable modes on the finite-amplitude dynamics for a fixed parameter setting are discussed in section 4. The results are used as a guide for determining the appropriate truncation level for the study of wavenumber transition and hysteresis. The nonlinear solutions as a function of basic flow instability are presented in section 5. Finally, section 6 concludes the description of the numerical experiments and provides further remarks.

2. The model and linear analysis

The model used here is identical to that in Chou and Loesch (1986b, hereafter referred to as CL)—that is, a quasigeostrophic model based on Eady (1949) with the addition of unequal Ekman dissipation at the top and bottom rigid boundaries. A continuously stratified fluid, rotating on an f plane, is contained in a channel, periodic in the zonal direction and bounded by vertical walls in the north and south. The basic state is a zonal flow of constant vertical shear—that is, λz in nondimensional form, where λ is the vertical shear and z is the height. This basic state yields a conservation of quasigeostrophic potential vorticity in the interior, while the vertical velocity pumped out of the Ekman layers specifies the boundary conditions at the top and bottom of the channel. The governing equation and boundary conditions for the nondimensional perturbation streamfunction ϕ are

$$\nabla^2\phi + S^{-1}\phi_{zz} = 0, \qquad (2.1a)$$

$$\phi_x = \bar{\phi}_{yt} = 0, \quad \text{at} \quad y = 0, 1 \qquad (2.1b)$$

$$\phi_{zt} = -\lambda z\phi_{xz} + \lambda\phi_x + \begin{Bmatrix} r_1 \\ -r \end{Bmatrix} S\nabla^2\phi - J(\phi, \phi_z),$$

$$\text{at} \quad z = \pm\tfrac{1}{2}, \quad (2.1c)$$

where the overbar represents a zonal average, $J(g, h) = g_x h_y - g_y h_x$ is the Jacobian describing the nonlinear advections of the flow, S is the (constant) stratification parameter, and r and r_1 are the Ekman dissipation associated with the lower and upper boundary, respectively (refer to CL for more details concerning the model). Note that the nonlinearity enters the problem only through the boundary conditions (2.1c).

The linear eigenvalue problem has been solved and discussed in detail in CL. Here, only the properties pertinent to the current study are presented. The wave solution is sought in the form of

$$\phi = F(z)e^{ik(x-ct)}\sin n\pi y, \qquad (2.2)$$

where k is the zonal wavenumber, n is an integer denoting the meridional mode, $F(z)$ is the vertical structure, and c is the (complex) phase speed. The linear growth rate kc_i as a function of wavenumber and vertical shear for the gravest meridional mode $n = 1$ is shown in Fig. 1 for $S = 0.1$, $r = 1$, and $r_1 = 0.1$. The

flow becomes unstable when λ exceeds the critical value of $\lambda_{c,\min} = 0.587$, where the linearly most unstable wave is $k = 3$. The sideband waves become unstable when the shear is slightly increased above $\lambda_{c,\min}$; that is, the shears for $k = 4$ and 2 are 0.630 and 0.645, respectively. A shortwave cutoff is present at $k = 7.72$ beyond which the waves are always stable. For the second meridional mode $n = 2$, only wavenumbers 1–5 are unstable, while the critical wave remains $k = 3$ with a critical shear of 2.18. For even higher meridional modes $n \geq 3$, all waves are stable. The critical shears for the unstable modes are listed in Table 1 for $S = 0.1$, $r = 1$, and $r_1 = 0.1$. The confinement of instability to long waves and low meridional modes is due to the constraint imposed on the vertical e-folding distance, which is inversely proportional to $[S(k^2 + n^2\pi^2)]^{1/2}$ [see CL, (2.8)].

Close examination of Fig. 1 reveals that as the flow becomes more supercritical the fastest growing wave gradually shifts to a shorter wave; for example, at $\lambda \sim 1.5$ the fastest growing wave becomes $k = 4$. As mentioned in the introduction, this poses certain important questions: Which wave dominates at finite amplitude as the flow becomes more supercritical? Will the dominant wave shift to a shorter wave as predicted by the linear theory? Or, will it shift to a longer wave as observed in the annulus experiment and weakly nonlinear theory?

Another question arising from the linear analysis is the effect of *stable* wave components in finite-amplitude equilibration. As the unstable waves grow, the self-interaction of these waves generates a correction to the mean state which, in turn, modifies the stability characteristics of the zonal flow. Also, the wave–wave interactions among the growing waves may have a positive contribution to the *nonlinear* growth of certain wave scales. The combined quasi-linear and nonlinear effects may then destabilize the linearly stable waves. This usually occurs during the initial spinup when the instability is strong and the feedback is intense. These stable waves may eventually decay to zero as the system reaches its final equilibrium state. However, regardless of how ephemeral and subtle these waves are, they may play a profound role in determining the final wave state since, as will be shown later, the final wave state depends not only on the physical parameters of the model but also on how the solution is approached in parameter space. Also, as indicated by Cehelsky and Tung (1987), the presence of small-scale waves provides a path for proper energy and vorticity cascades to the small scales where significant dissipative sinks are present. For the current parameter setting only 12 unstable wave modes were found ($k = 1$–7 for $n = 1$ and $k = 1$–5 for $n = 2$). It is not clear whether it is adequate to include only the unstable modes in the model, even just to *qualitatively* describe its finite-amplitude behavior. This will be examined by varying the

TABLE 1. Linear critical shear for the unstable wave components for $S = 0.1$, $r = 1$, and $r_1 = 0.1$.

	n	
k	1	2
1	1.031	4.694
2	0.645	2.652
3	0.587	2.182
4	0.630	2.287
5	0.747	3.666
6	0.976	stable
7	1.596	stable

zonal and meridional truncation levels, while keeping the model parameters at fixed values.

3. The spectral numerical model

As in CL, a spectral numerical method based on Fourier expansion is used to solve (2.1). The perturbation streamfunction, which satisfies the boundary conditions (2.1b), is represented by two truncated Fourier series

$$\phi = \sum_{m=1}^{M} \sum_{n=1}^{N} C_{mn}(z, t) e^{imkx} \sin n\pi y$$

$$+ \text{c.c.} + \sum_{l=1}^{L} \bar{C}_l(z, t) \cos l\pi y, \quad (3.1)$$

where the first series represents a wavelike streamfunction, the second series represents the correction to the mean flow, and c.c. represents the complex conjugate of the previous term. The vertical structures of the complex wave component C_{mn} and the zonally mean component $\bar{C}_l$ are solved directly from (2.1a) to yield

$$C_{mn} = A_{mn}(t) \cosh 2\mu_{mn}z + B_{mn}(t) \sinh 2\mu_{mn}z$$

$$\bar{C}_l = M_l(t) \sinh 2\alpha_l z + N_l(t) \cosh 2\alpha_l z,$$

where

$$\mu_{mn} = 0.5[S(m^2k^2 + n^2\pi^2)]^{1/2} \text{ and } \alpha_l = 0.5 S^{1/2} l\pi.$$

The resulting $2(M \times N + L)$ coupled first-order ordinary differential equations are integrated numerically in time using a fourth-order Runge–Kutta scheme. A transform method, which is based on the fast Fourier transform to compute the Jacobian terms in (2.1c), has been developed to replace the interaction coefficient method used in previous studies. This new algorithm increases the efficiency of the calculation and enables us to include enough wave harmonics in both the zonal and meridional directions to critically examine the effect of stable short waves in wave equilibration.

Unlike in the majority of the previous baroclinic instability studies by the author (Chou and Loesch 1986a,b; 1991), where the primary interest was on the linearly most unstable wave ($k = 3$), in the present

study the fundamental wavenumber is chosen as $k = 1$ to include the long waves and allow for both upscale and downscale energy transfers from the most unstable wave. The basic parameters chosen for the present study are fixed at $S = 0.1$, $r = 1$, and $r_1 = 0.1$, which are close to the atmospheric values according to CL. The nondimensional time step used is $\Delta t = 0.02$, which has been proven to be adequate for the present study. The remaining unspecified variable in (2.1) is the basic-state shear λ, which measures the baroclinicity of the system. Here, we define the supercriticality as the amount of shear exceeding the minimum critical shear; that is,

$$\Delta = \lambda - \lambda_{c,\min}.$$

Due to the meridional structure of the perturbation imposed by the sidewall boundary conditions, the system can be divided into $m + n = $ even and $m + n = $ odd subsets, which interact with each other indirectly through the mean flow. If the perturbation contains only one of the subsets initially, the other subset will remain zero for all time. To ensure that each subset has an equal opportunity to grow, the initial conditions are chosen such that there is at least one nonzero wave amplitude in each subset at the beginning of each integration.

4. Effect of stable wave components

Intuition may suggest that the inclusion of all unstable modes in the wave spectrum is sufficient to *qualitatively* describe the nonlinear wave evolution and, as more modes are included, the accuracy of the approximation may improve. To test this conjecture, a series of integrations is conducted using various truncation levels. The supercriticality is fixed at $\Delta = 1.2$ (i.e., $\lambda = 1.787$), which is unstable to the wave components with fundamental meridional mode $n = 1$, but is stable to the wave components with higher meridional modes (see Table 1). The initial conditions are $A_{21}(0) = A_{31}(0) = 0.001$.

When the wave field consists of only the (linearly) unstable components and the mean-flow correction is limited to the gravest meridional mode, that is, $(M, N, L) = (7, 1, 1)$, the solution grows out of bound due to the insufficient mean-flow representation to stabilize the system. Including more meridional harmonics in the mean field results in a damped vacillation consisting of a dominant wavenumber 3 and a weaker wavenumber 2. This is shown in Fig. 2a for the $(7, 1, 3)$ truncation. Note that waves that do not exist initially are not generated since the restriction to a single meridional mode in the wave field precludes wave–wave interactions. The nonlinear interactions in this case are limited to the self-interactions of wavenumbers 2 and 3, which contribute to the correction of the mean flow, and the interactions of the mean flow and wavenumbers 2 and 3, which contribute to the equilibration of each

wave. Because wavenumber 3 has a larger growth rate, it extracts most of the available potential energy from the zonal flow and contributes to the bulk of the mean-flow correction. In fact, the time evolution of wavenumber 3 is almost identical to the case in which wavenumber 3 is the sole wave in the system. The solution essentially remains the same for $L \geqslant 3$, indicating a fast-converging series of the mean flow when the wave field is limited to a single meridional mode.

The effects of *stable* wave components on wave equilibration are examined by systematically increasing the truncation level in the wave field, first in the meridional direction and then in the zonal direction. When higher meridional harmonics are included in the wave field, the wave–wave interaction becomes possible and energy can be transferred in both upscale and downscale directions. The energy transfer is most vigorous during the initial adjustment period when the instability is strongest. As shown in Fig. 2b for the $(7, 2, 3)$ truncation, all wave modes are generated through wave–wave interactions when the second meridional harmonics are included in the wave field. Here, wavenumber 3 reaches a steady state through a damped vacillation similar to the $(7, 1, 3)$ truncation. However, wavenumber 2, together with all other waves, grows initially but eventually decays to zero. The result remains the same when more mean field harmonics are included. As shown in Fig. 2c, the solution for the $(7, 3, 3)$ truncation changes drastically from the lower-order solutions. The interaction is strong at the initial stage, and the dominant wavenumber switches to wavenumber 2 after about 100 time units. The system eventually reaches a multiwave state, which vacillates chaotically. When the wave field is better resolved, most of the chaos disappears as is shown in Fig. 2d for the $(7, 5, 5)$ truncation.[1] The presence of "spurious chaos" indicates that the lower-order model does not have the proper channels through which energy can cascade upscale and enstrophy can cascade downscale (Cehelsky and Tung 1987). In the higher-resolution model, the chaotic behavior is limited to the initial adjustment stage when the waves are competing for the available potential energy released by the instability. Afterward, wavenumber 2 emerges as the sole survivor of the system and reaches a steady state.

A further increase in meridional resolution produces a similar solution with better approximation, except for the $(7, 11, 11)$ truncation,[2] where a *qualitatively* different behavior emerges. Instead of diminishing to zero, wavenumber 3 remains dominant for all time and

---

[1] Since the FFT algorithm uses only one meridional length for both wave and mean fields, it will be to our advantage to set $N = L$ in further calculations.

[2] The seemingly bizarre number used here is due to the FFT limit on the total length of transformation, *including the mean field*, to $2^p 3^q 5^r$, where $p \geqslant 1$, and $q, r \geqslant 0$.
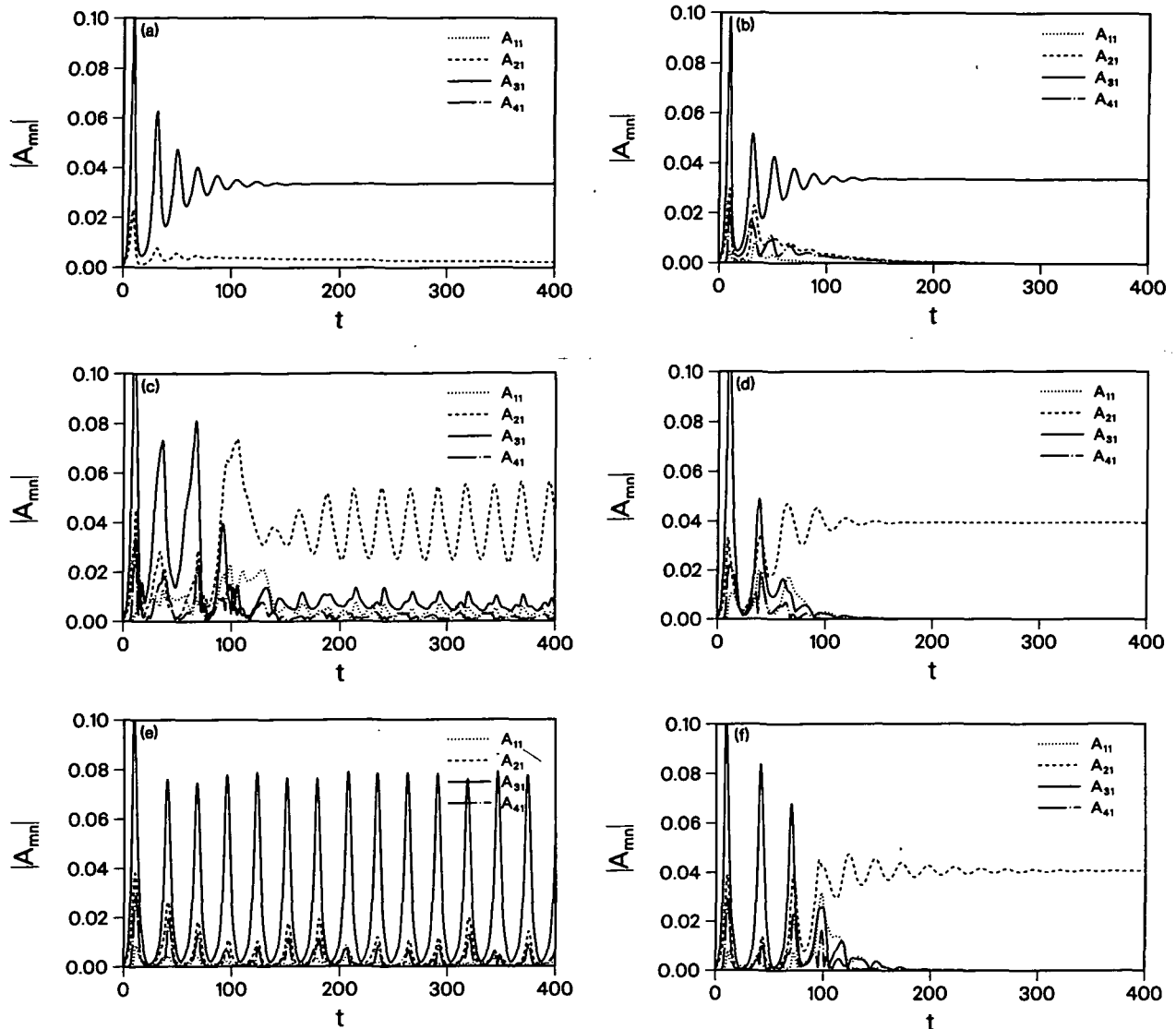
FIG. 2. Solutions for various meridional truncations when the zonal truncation is kept at $M = 7$: (a) $N = 1$, $L = 3$; (b) $N = 2$, $L = 3$; (c) $N = L = 3$; (d) $N = L = 5$; (e) $N = L = 11$; and (f) $N = L = 23$. The parameter setting is $S = 0.1$, $r = 1$, $r_1 = 0.1$, and $\Delta = 1.2$.

vacillates perpetually, while all other waves reach small but finite amplitude. This vacillatory mixed-wave state is shown in Fig. 2e. It was puzzling at first that the solution converged to a totally different attractor as the truncation level was varied. However, it will become clear later that the unexpected change in solution characteristics was due to the fact that in certain parameter ranges a dynamic system can possess more than one stable solution, which is sensitive not only to physical parameters and initial conditions, but also to numerical techniques such as truncation level and integration scheme.

In a chaotic dynamic system, a slight difference in initial condition can lead to a profound consequence in the final solution (Lorenz 1962). The

sensitivity to initial condition can be applied to the current study as follows. When started with an *identical* initial condition, the difference in truncation level creates a different solution immediately following the first time step. Its effect is continuously felt at subsequent time integrations, contributing to the further deviation of solution trajectory in phase space. In a system where several *stable* attractors exist, the trajectory may close in upon one of the possible attractors and render a different flow behavior when truncation level is varied. For reference, Fig. 2f provides the solution with meridional truncation $N = L = 23$, which has been proven to be adequate for the current zonal truncation $M = 7$.

To investigate the effect of *stable zonal* wave on wave equilibration, the meridional truncation is fixed at $N = L = 23$. When more zonal waves are included in the wave spectrum, the solution changes character again. This is shown in Fig. 3a for the $(9, 23, 23)$ truncation. As in the low zonal wave case, after a period of adjustment wavenumber 2 emerges as the dominant wave. However, unlike in Fig. 2f, it vacillates forever, while all other waves gradually attain finite (although small) amplitude, resulting in a mixed-wave vacillatory state. When zonal resolution of the model is increased to $M = 11$, wavenumber 3 replaces wavenumber 2 as the dominant wave and vacillates perpetually. This is shown in Fig. 3b for the $(11, 23, 23)$ truncation. In contrast to the dominant wavenumber 3 state in Fig. 2e, here all the other waves diminish to zero and the system reaches a single wave vacillatory state. A further increase in zonal resolution results in a mixed-wave vacillatory state with dominant wavenumber 2, which is not dissimilar to Fig. 3a. The final converged solution for $\Delta = 1.2$ is shown in Fig. 3c for the $(23, 23, 23)$ truncation.

Here, we demonstrate that in wave equilibration the higher stable modes (both meridional and latitudinal) serve not only to better approximate the model solutions, but also to determine which of the possible solutions is ultimately reached. Due to the chaotic nature of the transition period, a slight difference in solution trajectory at initial stage may lead to a completely different final state in a multiple equilibria system.

To determine the truncation level for further investigation, several integrations with various truncation levels were conducted. It is found from previous calculations that for the solution to converge properly, the meridional and zonal harmonics need to increase concurrently; that is, $M = N = L$ is required. Since it is nearly impossible to duplicate exactly the whole wave history from beginning to end due to the chaotic nature of the transition period, a strategy was adopted that compares only the final equilibrated state and circumvents the capricious behavior of the transition period. A control case was run with a high resolution, $(M, N, L) = (31, 31, 31)$, until the final equilibrium state was reached. The final state was then used as the initial condition for lower-resolution integrations. By comparing the equilibrium state of the control solution and the lower-order solutions, the optimal truncation level can be determined. The lowest truncation required to *qualitatively* approximate the converged solution was found to be $(9, 9, 9)$. Quantitatively, its solution is surprisingly accurate and lies within 2% of the control case. For higher-order calculations, the accuracy is increased to better than 1% for the $(17, 17, 17)$ truncation and about 0.1% for the $(23, 23, 23)$ truncation. To ensure proper convergence for higher supercritical cases, the $(23, 23, 23)$ truncation was chosen for the hysteresis study in the next section. This truncation has been proven to be more than adequate, since in the hysteresis
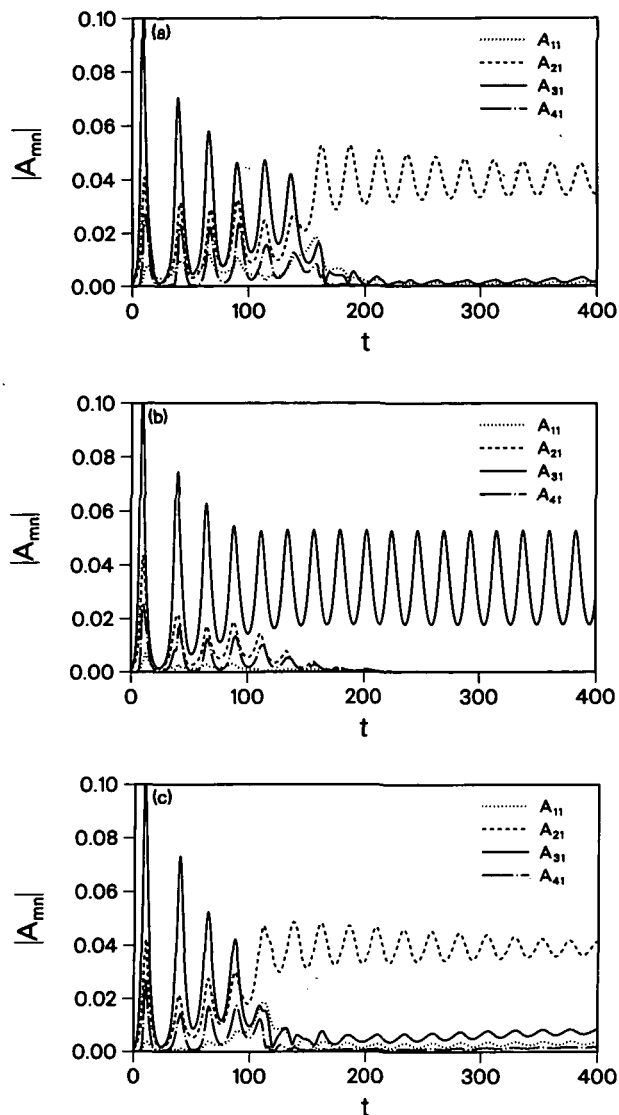

FIG. 3. Solutions for various zonal truncations when the meridional truncations are kept at $N = L = 23$: (a) $M = 9$, (b) $M = 11$, and (c) $M = 23$.

study the initial condition is never far from the converged solution due to the small increment in supercriticality. This truncation has a better resolution than that in CL, where the highest retained zonal wavenumber is 18 (for $k = 3$ and $M = 6$) with 12 meridional modes.

5. Hysteresis study

In this section, the model response is examined using a hysteresis approach; that is, the numerical integrations are carried out by stepwise varying one of the external parameters with a small increment, while using the equilibrated state of the previous parameter value as the initial state of the new run. If hysteresis exists,
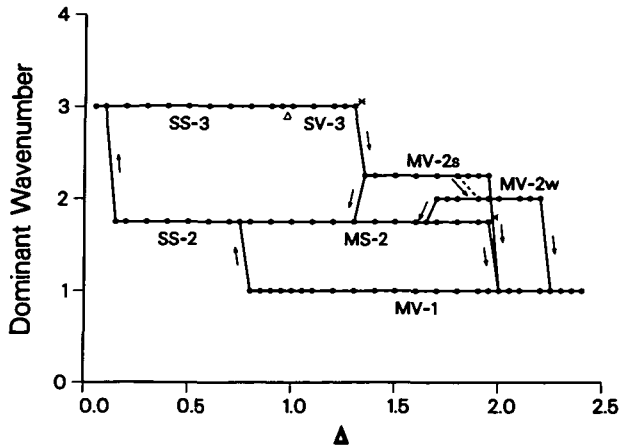
FIG. 4. Schematic diagram outlining the stable solutions of (2.1). Each solution branch is labeled by an alphanumeric symbol: the first letter denotes a single (S) or mixed (M) wave state; the second denotes a steady state (S) or vacillation (V), followed by the dominant wavenumber. An s or w is added on the MV-2 branches to indicate a strong or weak vacillation. The asterisk denotes an intermediate mixed-wave solution, and the arrow indicates the direction of increment.

the model response at a given parameter value will converge to a different fluid behavior when it is traversed from the opposite direction. The parameter chosen for this study is supercriticality Δ, and the numerical experiment starts from $\Delta = 0.1$ to $\Delta = 2.4$ then back to $\Delta = 0.05$. In general, the increment in Δ is 0.1, but is reduced to 0.05 when a change in solution characteristics is encountered to ensure that the new solution is genuine and not a numerical artifact caused by the imbalance of the flow at the initial stage.

As mentioned earlier, the wave spectrum consists of two nearly independent subsets, and if either one of them contains no initial energy or external forcing, that particular subset will remain zero forever. Therefore, when the final state of previous Δ contains only one subset, an additional amplitude of 0.001 is added in either A_{21} or A_{31} at the beginning of the new integration to ensure the inclusion of all possible growing modes. It was found in the subsequent experiments that the additional energy spreads to the rest of the subset in a matter of few time steps, if the instability so warrants.

The results of a hysteresis experiment are summarized in Fig. 4. The horizontal axis is the supercriticality Δ and the vertical axis is the final *dominant* wavenumber. Each solution branch is given by an alphanumeric symbol: the first letter denotes a single (S) or mixed (M) wave state, the second a steady state (S) or vacillation (V), followed by a number corresponding to the final dominant wavenumber. An s or w is added on the MV-2 branches to distinguish a strong vacillation from a weak one.

Figure 4 shows that at finite amplitude, instead of shifting to the faster growing shorter wave as predicted

by the linear stability theory, there is a succession of transition to longer waves as the flow becomes more supercritical. An example of wavenumber transition is given in Fig. 5 for $\Delta = 1.35$ where the flow behavior changes from a single wavenumber 3 state to a multi-wave state with dominant wavenumber 2. Note that the time-averaged amplitude reached by wavenumber 2 after transition is larger than that reached by wavenumber 3 before transition, indicating a higher efficiency in reducing instability by the longer wave. Before the threshold Δ for wavenumber transition is reached, at $\Delta = 1.3$ the flow goes through an intermediate state in which the equilibrated wave state consists of a full spectrum in a vacillatory manner (marked by an asterisk in Fig. 4). The presence of a precursory mixed-wave state in the transition from a *single-wave* state to another state of a longer dominant wave has also been observed by Hart (1981). However, in his study, transition through mixed-wave state and hysteresis is mutually exclusive; that is, the wavenumber transition either takes place through a mixed-wave state with no hysteresis or occurs abruptly in a hysteresis fashion without going through a mixed-wave state. In the present study the intermediate state is part of the hysteresis loop.

The reverse transition, that is, the transition to a shorter wave as supercriticality is decreased, takes place at a smaller Δ than the forward transition does,
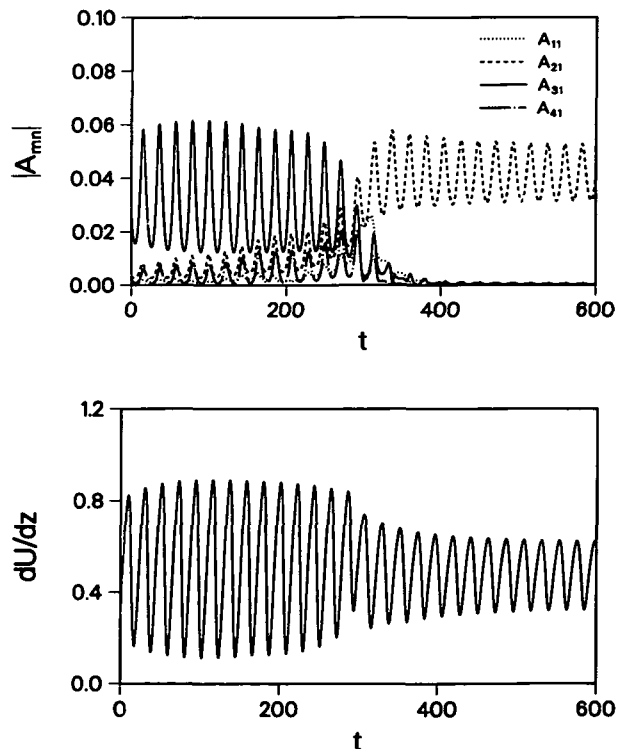

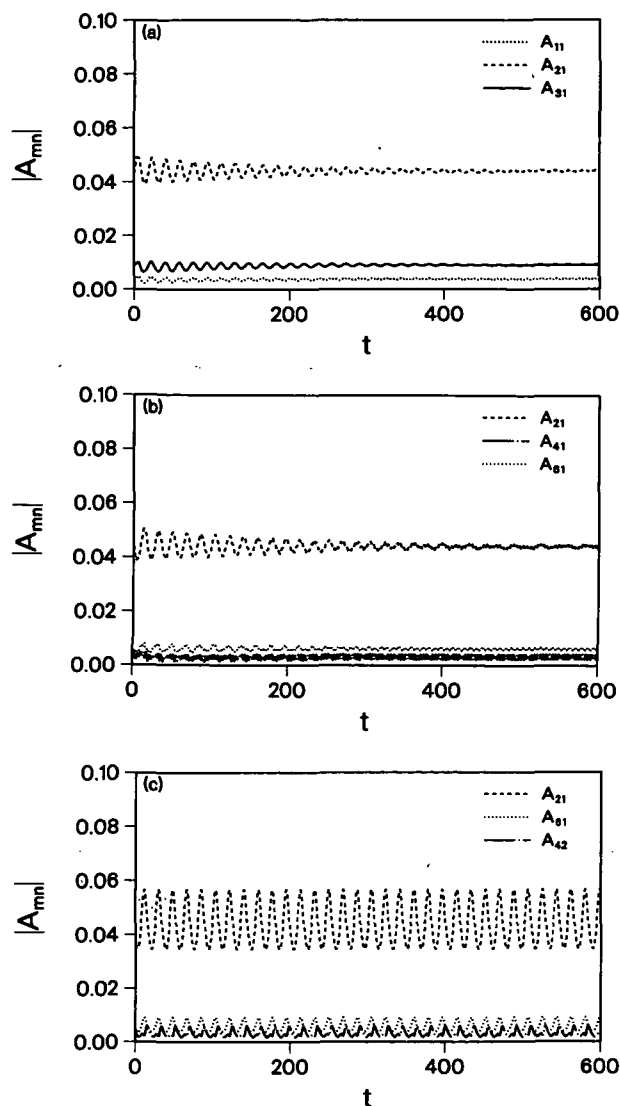FIG. 5. Amplitude and mean shear evolutions for $\Delta = 1.35$, showing a dominant wavenumber 3 to 2 transition.

FIG. 6. Three stable solutions with dominant wavenumber 2 for Δ = 1.8: (a) the MS-2 state, (b) the MV-2w state, and (c) the MV-2s state.

The three dominant wavenumber 2 solutions are illustrated in Fig. 6 for $\Delta = 1.8$, each with three leading wave components. All three solutions reach a multiwave state, but of different wave composition: the steady-state solution (the MS-2 solution) contains a full wave spectrum, the weak vacillation solution (the MV-2w solution) contains only even number zonal waves and their meridional harmonics, and the strong vacillation solution (the MV-2s solution) contains even less wave components in which the leading four wave components are $(m, n) = (2, 1)$, $(6, 1)$, $(4, 2)$, and $(2, 3)$. The vacillations found in the vacillatory wavenumber 2 states are quite regular in nature. The steady-state solution becomes vacillatory as the threshold Δ for wavenumber transition is approached (marked by an asterisk in Fig. 4 at $\Delta = 1.95$), whose amplitude variation lies between those of the strong and weak vacillation cases. The transition from each state to the dominant wavenumber 1 state occurs at a different Δ: $\Delta = 2$ for the MS-2 and SV-2 solutions, and 2.25 for the MV-2 solution.

Although only one dominant wavenumber 1 solution has been found, the MV-1 branch contains a variety of flow behaviors. The solution type and the leading equilibrated amplitudes with their vacillation range are illustrated in Fig. 7 for $0.8 \leqslant \Delta \leqslant 1.6$. In the first chaotic region ($0.8 \leqslant \Delta \leqslant 0.85$), the wave state displays a low-frequency variability, where the long waves (waves 1 and 2) vacillate with longer periods than the shorter waves (Fig. 8). The vacillation becomes less vigorous as Δ is increased, and at $\Delta = 0.9$ the vacillation of wavenumber 1 becomes so weak that it appears to reach a steady state, while wavenumber 3 vacillates regularly (the range of amplitude vacillation is shown in Fig. 7). (Although the terms regular vacillation and double-period vacillation are used here, they nevertheless contain a low-level noise.) When Δ is further increased to $\Delta = 0.95$, a different flow behavior starts to emerge (the A2 solution in Fig. 7). Here, the flow behavior changes aperiodically between two dis-

demonstrating a hysteresis behavior. Unique solutions exist only when the flow is weakly supercritical ($\Delta \leqslant 0.1$) or strongly supercritical ($\Delta \geqslant 2.25$), while multiple stable solutions prevail in the intermediate supercritical cases. Most notably, for $0.8 \leqslant \Delta \leqslant 1.3$ there exists three stable solutions, each with dominant wavenumber 1, 2, and 3, respectively, while for $1.7 \leqslant \Delta \leqslant 1.95$ there are four stable solutions: a dominant wavenumber 1 state and three dominant wavenumber 2 states, each with different wave characteristics. It is not clear whether all of the possible solutions in the parameter range have been found because the MV-2w state would have been totally missed if the finer Δ increment of 0.05 were used exclusively throughout the study.
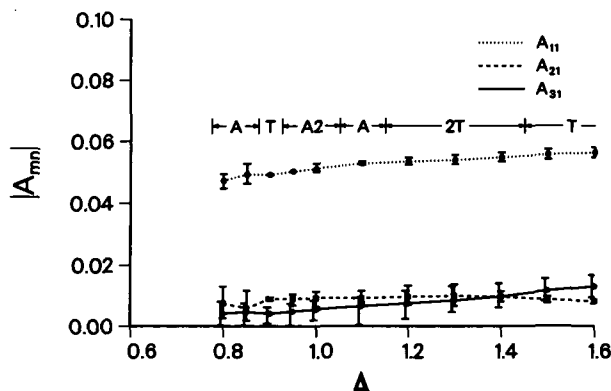

FIG. 7. Solution type and leading final amplitudes for the MV-1 solutions. The I-bar indicates the range of vacillation.
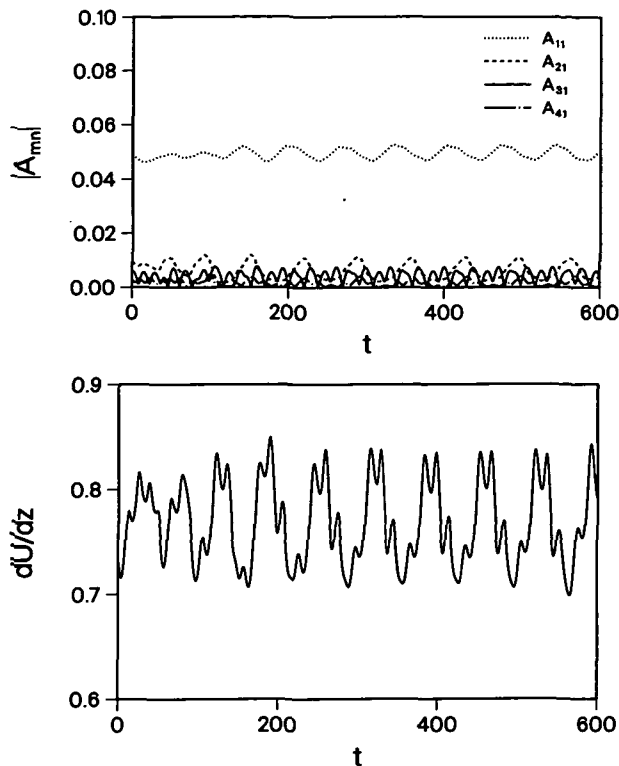
FIG. 8. Amplitude and mean shear evolutions for $\Delta = 0.85$, showing a chaotic vacillation with two predominant frequencies.

tinct states: a relatively regular vacillation and a chaotic vacillation. As illustrated in Fig. 9, the chaotic vacillation is characterized by a slightly elevated dominant wave amplitude, a doubled period for the shorter waves, and a weaker zonal shear at the center of channel, when compared to the regular vacillation. The behavior of switching aperiodically between two unstable attractors has also been observed by Lorenz (1990) in the form of interannual variability, and by Reinhold and Pierrehumbert (1982) in the form of multiple weather regimes, except here it is obtained strictly through the nonlinear baroclinic dynamics without the introduction of externally imposed forcing, such as seasonally varying heating or topographic forcing. The switch between two states becomes less pronounced as Δ is further increased, and at $\Delta = 1.1$ the chaotic vacillation appears again. At $\Delta = 1.2$, the chaotic vacillation coalesces to a double-period vacillation, which lasts until $\Delta = 1.4$ before transforming to a single-period vacillation. At this point, wavenumber 3 overtakes wavenumber 2 as the second most dominant wave, while wavenumber 1 still remains most dominant. At $\Delta = 2.35$, this vacillation starts to modulate with a long-period (~ 100 time units) oscillation and the solution takes a form of chaotic vacillation, which becomes more vigorous as Δ is further increased.

The MV-1 solutions obtained so far seem to indicate three possible routes to chaos: through an abrupt change in flow characteristics (from $\Delta = 0.9$ to 0.85 and $\Delta = 2.3$ to 2.35); through a multiple-regime stage where chaotic and regular vacillations appears alternatively (from $\Delta = 0.9$ to 1.05); and through a period doubling (from $\Delta = 1.5$ to 1.05). A detailed investigation of the routes to chaos requires a smaller increment in Δ, which is beyond the scope of the present study.

Figure 10 illustrates the time-averaged zonally mean shear at the center of the channel for the solution branches shown in Fig. 4. In general, the solution with a longer dominant wave equilibrates to a larger mean shear and prevails at larger values of Δ. For a given dominant wavenumber, the mean shear decreases as Δ is increased until a minimum is reached and then increases with Δ. For example, on the SS-3/SV-3 solution branch the zonally mean shear decreases from near the critical shear (0.587) for $\Delta = 0.05$ to a minimum of 0.424 at $\Delta = 0.8$ and then increases to 0.507 at $\Delta = 1.3$ before it switches to the SV-2 state. The corresponding time-averaged amplitude for the SS-3/SV-3 branch is given in Fig. 11. The time-averaged wavenumber 3 amplitude increases rapidly with Δ when Δ is small, levels off when Δ becomes larger, and starts to decrease after $\Delta = 1.2$. This indicates that wavenumber 3 becomes less effective in removing the imposed instability as Δ is increased toward the threshold Δ. Because longer waves can prevail at a higher equilibrated shear, the natural selection process favors the transition to a longer wave state when the short wave becomes incapable of neutralizing the imposed instability.

6. Conclusions and further remarks

A continuously stratified quasigeostrophic model has been used to investigate the wavenumber transition and hysteresis in unstable baroclinic flows. It is found that as the flow becomes more supercritical, the final dominant wavenumber may not be the linearly fastest growing wave, but will shift to a longer wave. In certain parameter ranges, the realized finite amplitude state is not uniquely determined by the external parameters, but also depends on the direction the solution is traversed in parameter space, thus, displaying a hysteresis behavior. Once a flow is established at a given point in the parameter space, it will remain unchanged until a critical value of the imposed parameter is reached for the onset of another state. Within the hysteresis range, multiple stable solutions are possible and each solution constitutes a branch of several intertwined hysteresis loops. In contrast to forced wave cases (Reinhold and Pierrehumbert 1982; Lorenz 1990), it is shown here that multiple weather regime or transitive variability can be found strictly in a thermally driven baroclinic system without the externally imposed forcing.
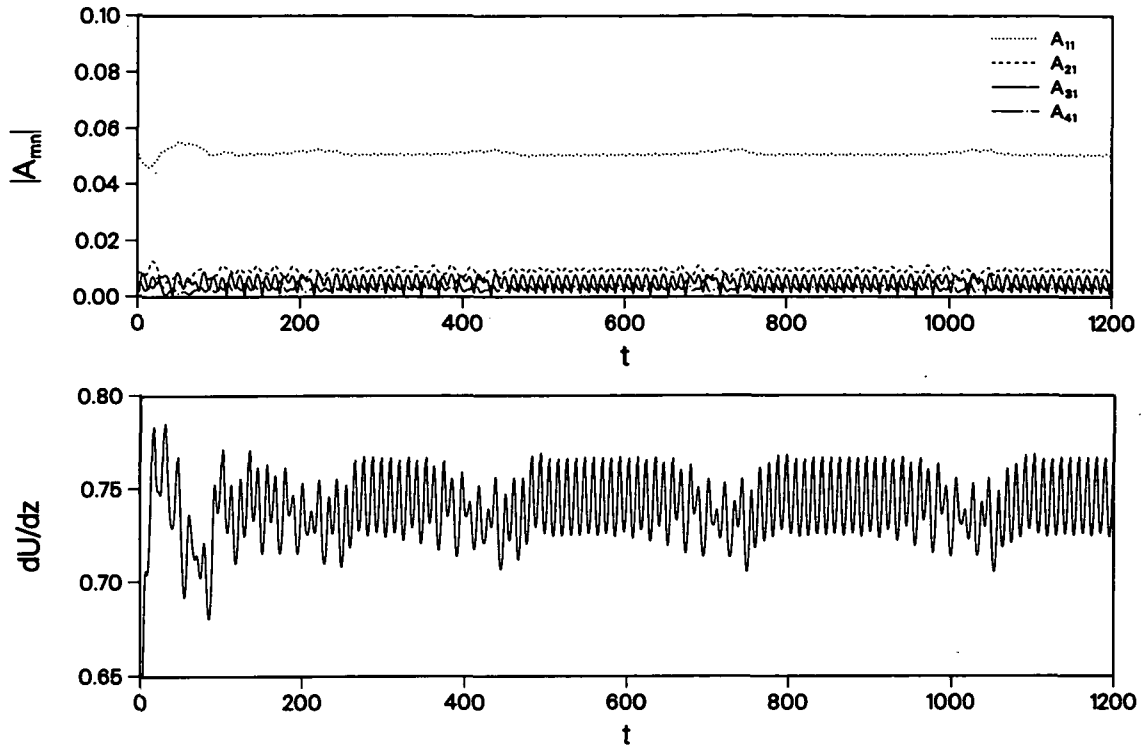
FIG. 9. Amplitude and mean shear evolutions for $\Delta = 1$, showing an aperiodic switch between two distinct states.

During the course of the investigation it is also found that, other than the initial condition discussed in the previous section, the finite-amplitude state of a baroclinic flow at a given parameter setting is also sensitive to several other factors such as truncation level and numerical techniques.

As discussed in section 4, within the hysteresis range the finite amplitude solution may reach a different flow state when a different truncation level is used. If the prescribed truncation level is high enough, the finite-amplitude state may converge to one of the stable solutions, but if the truncation level is low, the finite-amplitude state may approach a spurious solution due to insufficient wave components for energy and enstrophy cascade. A preliminary experiment, conducted with an $M = 6$ and $N = L = 12$ truncation, shows two separate hysteresis loops: a wavenumber 3 to 2 transition loop in $0.1 \leqslant \Delta \leqslant 0.3$ and a wavenumber 2 to 1 transition loop in $0.8 \leqslant \Delta \leqslant 1.75$. Single-wave steady states are always observed on the first loop, while single-wave steady states prevail for $\Delta \leqslant 1.2$ on the dom-
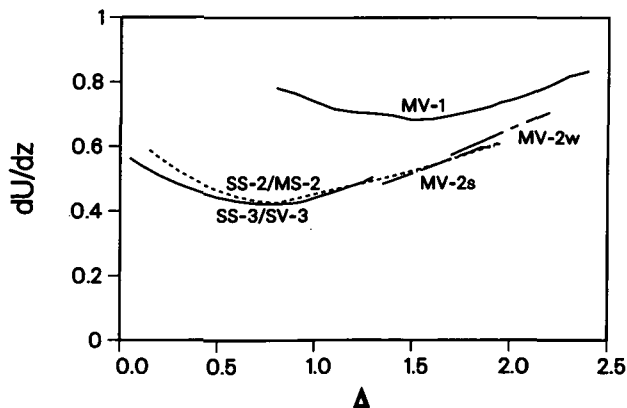

FIG. 10. Time-averaged equilibrium mean shear at the center of the channel for the solution branches shown in Fig. 4.
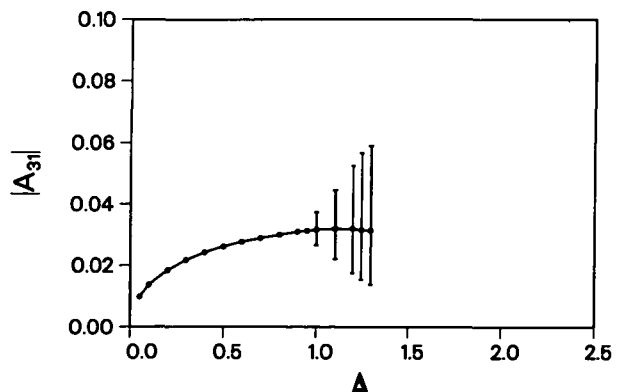

FIG. 11. Time-averaged amplitude for the dominant wavenumber 3 solution branch. The I-bar indicates the range of vacillation.

inant wavenumber 2 branch and mixed-wave vacillatory states prevail in the rest of the second loop. Compared to Fig. 4, the dominant wavenumber 3 in the lower truncation case exists in a much smaller supercriticality range and only one dominant wavenumber 2 branch was ever found so that no more than two solutions are possible at a given supercriticality. The sensitivity of solution to truncation level indicates that the low-resolution model should be used with caution, especially when applied to strongly nonlinear flows.

The presence of multiple solutions also makes the finite-amplitude solution sensitive to the numerical method used, especially when starting with arbitrary initial amplitudes or when the parameter setting is near the transition point in the regime diagram. For example, using a moderate truncation level ($M = 6$, $N = L = 12$) with initial conditions $A_{31}(0) = A_{21}(0) = 0.001$, the solution for $\Delta = 1.2$ converges to a dominant wavenumber 2 state. However, the interaction coefficient method yields a damped vacillation, while the transform method yields a perpetual vacillation. The sensitivity to numerical method is also observed in a numerical model of the baroclinic annulus when different finite difference schemes are used (Lu et al. 1994). To a lesser degree, perhaps, the finite-amplitude state may also depend on a time step used for integration, and the inherent architecture and round-off error of the computer used, especially when an arbitrary initial condition is used.

The presence of multiple solution in a quasigeostrophic system raises a question of the predictability of a climate system, just as the presence of chaos does of the predictability of the weather. The sensitive dependence of the long-term equilibrium state (i.e., climate) on initial conditions and numerical techniques may pose a problem in climate prediction using a general circulation model (GCM), since it is not clear whether the GCM solutions in the parameter range of realistic atmospheric situation are unique. The increased sophistication in GCM may act to "lock" in the system to a unique solution, but this argument remains illusive and further investigation is required. The hysteresis approach used in the present study can be applied to a GCM, but it may be prohibitively expensive at this moment. A more feasible alternative is to increase the complexity of the current model to include more realistic physical mechanisms, such as seasonal variation, land–sea contrast, and/or topographic forcing. This approach is currently under investigation.

REFERENCES

Buzyna, G., R. L. Pfeffer, and R. Kung, 1978: Cyclic variations of the imposed temperature contrast in a thermally driven rotating annulus of fluid. *J. Atmos. Sci.,* **35,** 859–881.

Cehelsky, P., and K. K. Tung, 1987: Theories of multiple equilibria and weather regimes—a critical reexamination. Part II: Baroclinic two-layer models. *J. Atmos. Sci.,* **44,** 3282–3303.

Chou, S.-H., and A. Z. Loesch, 1986a: Supercritical dynamics of baroclinic disturbances in a free-surface model. *J. Atmos. Sci.,* **43,** 285–301.

——, and ——, 1986b: Supercritical dynamics of baroclinic disturbances in the presence of asymmetric Ekman dissipation. *J. Atmos. Sci.,* **43,** 1781–1795.

——, and ——, 1991: Supercritical baroclinic disturbances under the influence of topography. *J. Atmos. Sci.,* **48,** 2461–2475.

Drazin, P. G., 1972: Nonlinear baroclinic instability of a continuous zonal flow of viscous fluid. *J. Fluid Mech.,* **55,** 577–587.

Eady, E. T., 1949: Long waves and cyclone waves. *Tellus,* **1,** 33–52.

Fein, J. S., 1973: An experimental study of the effects of the upper boundary condition on the thermal convection in a rotating, differentially heated cylindrical annulus of water. *Geophys. Fluid Dyn.,* **5,** 213–243.

Hart, J. E., 1981: Wavenumber selection in nonlinear baroclinic instability. *J. Atmos. Sci.,* **38,** 400–408.

Lorenz, E. N., 1962: Deterministic nonperiodic flow. *J. Atmos. Sci.,* **20,** 130–141.

——, 1990: Can chaos and intransitivity lead to interannual variability? *Tellus,* **42A,** 378–389.

Lu, H., T. L. Miller, and K. A. Butler, 1994: A numerical study of wavenumber selection in the baroclinic annulus flow system. *Geophys. Astrophys. Fluid Dyn.,* **75,** 1–19.

Miller, T. L., and K. A. Butler, 1991: Hysteresis and the transition between axisymmetric flow and wave flow in the baroclinic annulus. *J. Atmos. Sci.,* **48,** 811–823.

Pedlosky, J., 1970: Finite amplitude baroclinic waves. *J. Atmos. Sci.,* **27,** 15–30.

——, 1981: The nonlinear dynamics of baroclinic wave ensembles. *J. Fluid Mech.,* **102,** 169–209.

Reinhold, B. B., and R. T. Pierrehumbert, 1982: Dynamics of weather regimes: Quasi-stationary waves and blocking. *Mon. Wea. Rev.,* **110,** 1105–1145.